WPS1-PR(18) 21331

V.E. Moiseenko et al.

Features of regular discharges in Uragan-3M torsatron

Preprint of Paper to be submitted for publication in
Plasma Physics and Controlled Fusion

This work has been carried out within the framework of the EUROfusion Consortium and has received funding from the Euratom research and training programme 2014-2018 under grant agreement No 633053. The views and opinions expressed herein do not necessarily reflect those of the European Commission.

Features of regular discharges in Uragan-3M torsatron

V E Moiseenko, A N Shapoval, A V Lozin, V V Nemov, V N Kalyuzhnyj, M M Kozulya, R O Pavlichenko, V G Konovalov, A E Kulaga, Yu K Mironov, V S Romanov, N V Zamanov, V N Bondarenko, Yu V Kovtun, I E Garkusha

Institute of Plasma Physics, National Science Center 'Kharkov Institute of Physics and Technology', Kharkiv, Ukraine

E-mail: moiseenk@kipt.kharkov.ua

Abstract

The Uragan-3M device is equipped with two antennas which are fed by RF power with the frequency below ion cyclotron. The frame antenna was used for pre-ionization and the three-half turn (THT) antenna makes plasma heating. In this experimental series, the radial profiles of C III, O V and C V optical lines intensity and the second cyclotron harmonic emission are measured using a pulse-by-pulse technique. The results of these measurements and Biot-Savart calculations of the Uragan-3M magnetic configuration could be explained by existence of a small central area with relatively high electron temperature and good plasma confinement surrounded by a zone where the electron temperature and confinement are worse. The relatively low average electron temperature and high RF power needed to sustain plasma are the consequences.

1. Introduction

The Uragan-3M [1], a small-size device of stellarator (torsatron) type, is equipped with two antennas, frame [2] and tree-half-turn (THT) [3], which are fed by RF power with the frequency below ion cyclotron. They heat mainly plasma electrons via absorption of the slow wave owing to the Landau mechanism. The slow wave is exited both directly and through the wave conversion at the Alfvén resonance layer [4]. The direct excitation of the slow wave by the frame antenna is more efficient [5,6] and, therefore, it is able to make plasma production [7]. The THT antenna is more oriented to the Alfvén resonance excitation and is used for plasma heating. Both antennas are of small-size. They generate waves with wide $k_{\|}$ spectrum. For this reason, a number of Alfvén resonances are present in plasma column. The periphery located Alfvén resonances are not useful since they cause heating of the plasma edge. The THT antenna excites them less than the frame antenna [3].

In the series of the experiments that are analyzed here, the low power pulse of the frame antenna goes first. It is used just to create plasma. After this, the powerful pulse of the THT antenna is provided. Such a regime of heating is briefly described in [8].

In this experimental series, the attention is paid to the radial distributions of the spectral line emission of the impurities (chord distribution) and the electron cyclotron emission distribution. The information on the radial profile is discussed in sense of the special features of plasma confinement in Uragan-3M.

2. Experimental setup and diagnostic methods

The Uragan-3M (U-3M) device is the three-turn ($l = 3$) torsatron with nine periods ($m = 9$) of helical magnetic field. The torus major radius is $R_{tor} = 100$ cm, an average last-closed magnetic-surface radius is $\bar{a} = 12$ cm (average plasma minor radius) and the magnetic field ranges up to 1 T. The rotational transform at the plasma boundary is $\iota(a)/2\pi \approx 0.3$. The whole magnetic system including the helical coils, the vertical field coils and the support, is placed into a large vacuum tank, 5 m in diameter and 3.6 m high, which volume (70 m^3) by 200 times exceeds the plasma confinement volume. The distinctive feature of this device is the magnetic configuration with a natural divertor.

During this experimental series, the toroidal magnetic field at the toroidal torus axis was $B = 0.7$ T, the hydrogen pressure was $p \approx 10^{-3}$ Pa. The initial plasma was created and heated with the frame antenna (FA) powered up by the Kascad-1 (K-1) generator (frequency is 8.6 MHz; power supply is $P_{RF} \leq 50$ kW while anode voltage is below 5.0 kV; RF pulse is set from 10^{th} ms to 14^{th} ms). The RF power for the THT antenna was fed from the Kascad-2 generator (K-2: frequency is 8.7 MHz; anode voltage is 9.0 kV; RF pulse is set from 14^{th} ms to 30^{th} ms) immediately after the end of the K1 generator pulse. The RF power is calculated using measured amplitudes of the forward and backward cable waves in the feeder line.

The time dependence of the average electrons plasma density was measured using a microwave interferometer. The operational frequency of this superheterodyne interferometer equals to 140 GHz [9]. The corresponding critical density for this frequency is $2.43 \cdot 10^{14}$ cm^{-3}. Probing a plasma provided by the ordinary polarized wave along a single vertical chord in the symmetric cross-section A2 passing through the plasma center (see Fig. 1).

The average electron temperature is evaluated from the soft X-ray measurements. The measurement of the electron cyclotron emission (ECE) was used to the determination of the electron temperature profile. ECE system operated a single channel heterodyne radiometer at second harmonic of the extraordinary wave [10-12]. The frequency range is 32-40 GHz. Radiation from the plasma is collected by a conical horn antenna that was oriented perpendicular to the magnetic field lines and is located on the part of a low magnetic field (see Fig. 1, cross-section D3). Under similar plasma conditions radial the electron temperature profile could be obtained if we combine data from series of plasma discharges only (pulse-by-pulse). In optically thick plasmas, the intensity of the ECE radiation is proportional to the local electron temperature. For U-3M plasmas, the case is of an optically not dense plasma ("grey plasma") and correction for the radiative temperature must be applied [10, 11]. Thus, entire electron temperature profile data has to be corrected with the optical depth factor.

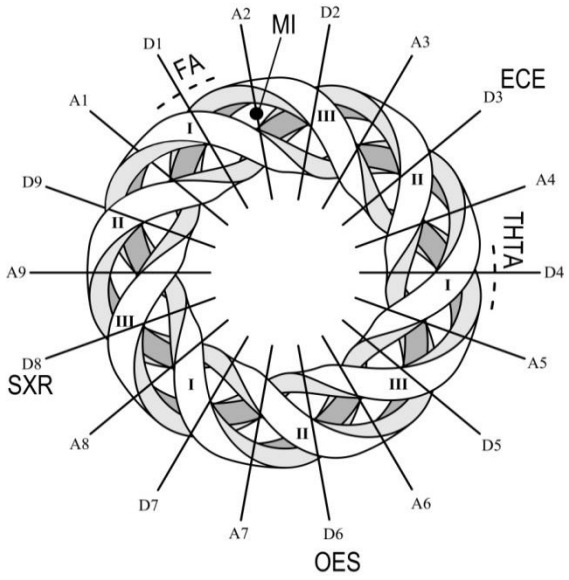

Figure 1. Scheme of Uragan-3M diagnostics: MI - microwave interferometer, ECE - electron cyclotron emission; OES - optical emission spectroscopy; SXR - soft X-ray. Two antennas: frame (FA) and tree-half-turn (THTA). Helical coils I, II, and III of the magnetic field. The poloidal cross-sectios are denoted by numbered characters.

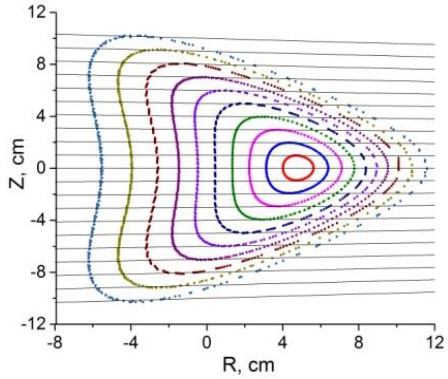

Figure 2. Scheme of measurement radial chord distribution

The plasma composition was analyzed with time resolved optical emission spectroscopy (OES). Time-resolved OES was carried out using a monochromator-spectrograph SOLAR TII (SOL instruments Ltd) model MS7501i (Cherny–Turner optical scheme) with a photomultiplier tube. The vertical scanning was performed with 21 chords (see Fig. 2) in cross-section D6 (see Fig. 1). The chord distribution are measured using a pulse-by-pulse technique. The numerical method of reconstruction the radial distribution was discussed in [13] for the non-symmetrycal case, so-called, Pearce approach [14] (solution of the system of linear algebraic equations). For the axially asymmetric magnetic surfaces in the U-3M the approach of Pearce was realized in [15]. The reconstruction assumes that the density of the ions is constant at the same magnetic surface see Fig. 2 (without taking into account the island structures). Besides, it was supposed that presence of the plasma does not distort essentially the configuration of the vacuum magnetic surfaces.

3. Experimental results

The RF power, the chord averaged plasma density and the average electron temperature evolution for such a discharge is displayed in Figure 3. A small power of K-1 generator is sufficient to create plasma with density $\bar{n}_e \approx 3 \cdot 10^{12}$ cm^{-3}. At the beginning of the K-2 pulse the plasma density slightly decreases and then slowly ramp up to the end of the RF pulse. The ramp up is accompanied by some decrease in RF power. After termination of the RF heating the plasma density jumps up by approximately 30 % to $\bar{n}_e \approx 6.5 \cdot 10^{12}$ cm^{-3}. This jump could be explained by some increase in plasma confinement without influence of RF heating. After this the plasma density slowly decays with characteristic time of 10 ms. The average electron temperature is small enough and does not show noticeable variation during the pulse.

Figure 4 shows the temporal evolution of the radial profiles of the electron radiation temperature T_e^{rad}. The radial flux coordinate used in Figures is a label of the magnetic surfaces. It is calculated as $\langle r \rangle = \sqrt{S/\pi}$, where S is the area surrounded by the magnetic surface. In the magnetic island region the coordinate is interpolated. The emission is strongly centrally localized. After RF heating turn-off it decays quickly, but less rapidly at the central plasma area.

The H_γ chord distribution is given in Figure 5. The volumetric emission of H_γ appears by the end of the frame antenna pulse. It accompanies plasma production. Several electron collision processes could be responsible for the H_γ emission. Among them the excitation of atomic hydrogen and dissociative excitation of the hydrogen molecules and molecular ions are. The relative intensity of Balmer series lines is different for atoms and molecules [16]. The study made in Reference 17 indicates that there is a domination of the lines produced by the dissociative excitation in U-3M discharges. The location of the emission at the plasma edge is due to the slowness of hydrogen molecules which are ionized and dissociated before reaching the plasma core. The atoms have manly Frank-Condon energies, 2-3 eV, and are much faster than the molecules. They penetrate deeper into the plasma core.

Immediately after the start of the K-2 pulse the intensity of H_γ decreases for short time. This could happen owing to the plasma density decrease near the plasma column edge. Some decrease of the line averaged electron density can be seen at Figure 3. but it is fairly small. More probable explanation is the electron temperature decrease at this time moment. This may happen if the power deposition is more central during the THT antenna pulse. The restoration of the H_γ emission is due to the heat transport from the central region to the plasma edge.

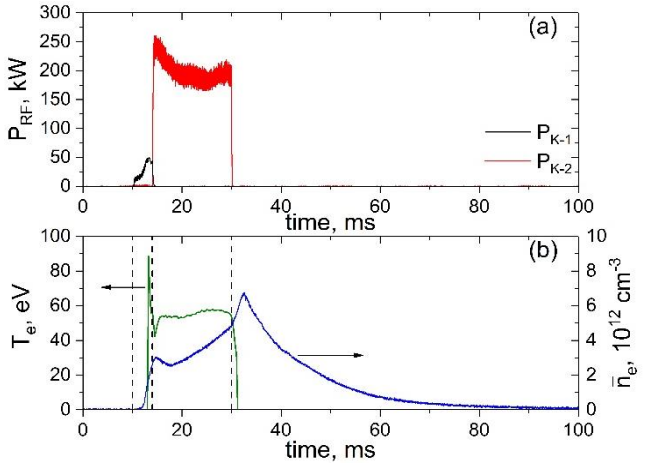

Figure 3. Time evolutions of RF powers $P_{K\text{-}1}$ (K-1), $P_{K\text{-}2}$ (K-2) launched to plasma (a) and average plasma density $\bar{n}_e$, average electron temperature T_e (b). The vertical lines show time of start and termination of RF power.

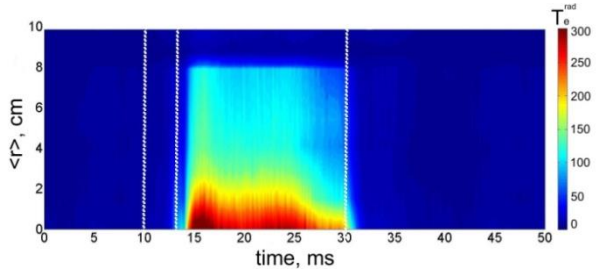

Figure 4. Temporal evolution of the radial profile of the radiation electron temperature.

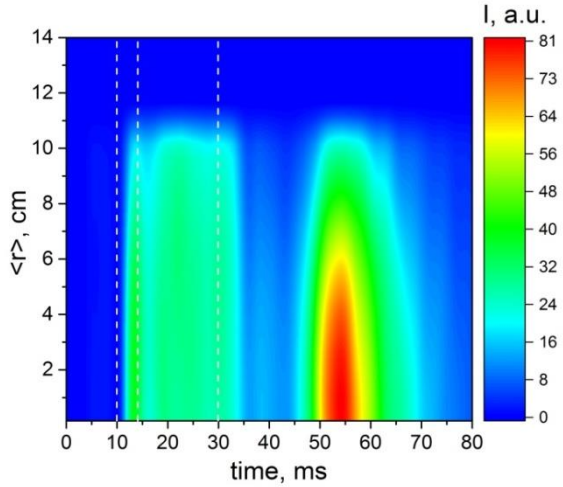

Figure 5. Time evolution of H_γ chord distribution.

There is a dip of emission intensity in the central area of the plasma column that indicates lower hydrogen recycling in this place. This can be caused by flattening plasma density profile and, as a result, decreasing diffusive flow of plasma particles from the centre to the border or by better plasma confinement in the central region. The central peak of H_γ emission that appears 20 ms after the RF heating turn-off witnesses against the profile flattening. After turn–off of the RF heating H_γ emission continues for 2-3 ms, and the plasma density increases by 40 %.

Presence of the carbon impurity is typical for fusion plasma discharges. Before analysis of the C III emission data some notes should be made. To make C^{2+} from a C^{+} ion the energy amount of 24.38 eV must be spent and, the energy threshold of C^{2+} excitation is 18.1 eV. The cost of transition of C^{2+} to the next ionization state is 47.86 eV. The above energy values indicate that at plasma with electron temperature of 50 eV and higher the ion state C^{2+} is transient.

C III line emission radial profile is displayed in Figure 6. The emission appears by the end of the frame antenna (pre-ionization) pulse. It is periphery located and has a maximum at $\langle r \rangle \approx 7$ cm. Some emission exists beyond the plasma confinement volume in the scrape-off layer plasma. As well as H_γ line, C III line intensity reduces after start of the THT antenna pulse and shortly after restores. The periphery emission increases to the end of the pulse that could be explained by the plasma density increase. During the whole discharge the minimum of the emission is kept at the plasma centre and the nearby area $\langle r \rangle < 3$ cm. After termination of the RF heating a powerful recombination peak comes. It has a major maximum at $\langle r \rangle \approx 7$ cm. The major amount of carbon impurity is confined around this location. Another smaller maximum is in the plasma column centre. The major maximum appears with the delay of 2-3 ms. For the central area, the delay is bigger, 4 ms. This means that in the central area the carbon is in higher ionization state than at the plasma periphery.

The oxygen impurity is also present in the discharge. The O V line emission is investigated in this experimental series. The O^{4+} ion characteristics are the following: the energy necessary for obtaining the O^{4+} ion from a lower ionization state is 77.39 eV, the excitation and ionization thresholds are 72.27 eV and 113.87 eV correspondingly. For this ion the magnitudes of the thresholds are more than 2 times higher than for C^{2+} ion.

The dependence of the O V emissivity in time is displayed in Figure 7. In the central zone of the plasma column O V emission appears at low level by the end of the frame antenna pulse and does not exceed this level to the THT antenna pulse end. After the RF power termination, with few milliseconds of delay, the strong narrow recombination peak comes indicating that the majority of the oxygen accumulated is in higher ionization state in this area.

In outer part of the plasma column the behaviour of O V emission is different. It appears during THT antenna pulse, acquires high intensity that increases in time, and also widens the light emitting area. After shut down of the RF heating the emission decreases, more rapidly near plasma edge. The whole picture of the O V emission indicates that the electron temperature is higher than the O^{4+} ionization threshold in the central area of the plasma column and lower than it at the remaining plasma part.

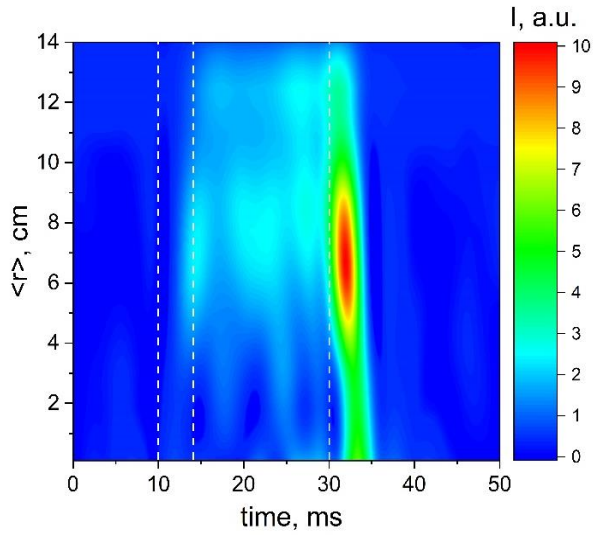

Figure 6. Time evolution of C III emissivity radial profile (wavelength is 229.6 nm).

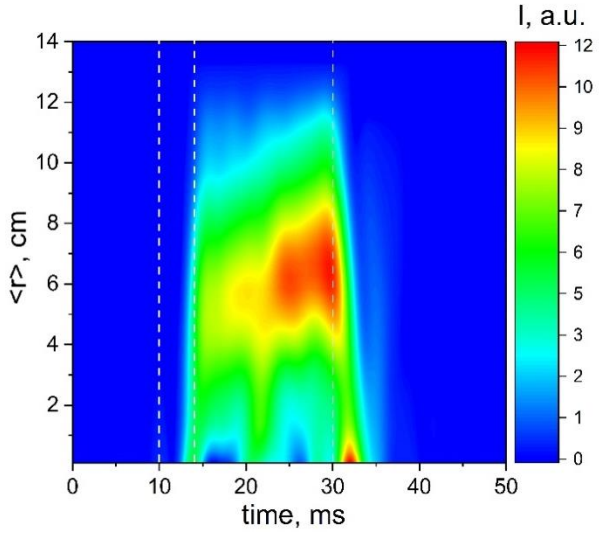

Figure 7. Time evolution of O V emissivity radial profile (wavelength is 278.1 nm).

The last impurity analyzed for luminosity is the ion C^{4+} (see Fig. 8). The threshold to create it from the previous ionization state is 64.48 eV, the excitation and ionization thresholds are 278.1 eV and 392 eV. Because of high excitation threshold this impurity ion can radiate efficiently only in plasma with electron temperature higher than 100 eV.

In the experiments, during the whole RF heating pulse, C V emission is observed only near the plasma column centre. It appears on the magnetic axis after some delay which is due to cascade ionization mechanism of creation of C^{4+}. During the pulse the intensity of the emission rises continuously and the location of the emission widens. However, the emission does not step out the central zone. There is no strong recombination peak after the end of the RF heating pulse. This character of the emission confirms the assumption on the high electron temperature in the central zone and low in the remainder part of the plasma column.

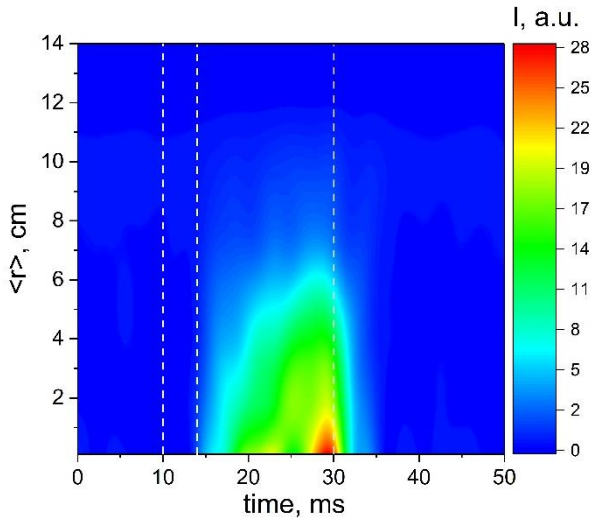

Figure 8. Time evolution of C V emissivity radial profile (wavelength is 227.1 nm).

4. Discussion of experimental results

The measurements of spectral line emission profiles suggest on existence of two areas with different electron temperatures. In the small near-axis area $\langle r \rangle < 3$ cm the electron temperature is high and in surrounding plasma it is small. This is confirmed by the ECE measurements. The strong peaking of the electron temperature cannot be explained by central localization of plasma heating only. Radial variation of the thermal conductivity may describe this fact. So, the confinement in the central zone is better than in the surrounding area of plasma confinement volume. Smallness of the energy confinement time can be explained by low ratio (order of ten) of the volumes of the hot kernel and cold surrounding plasma. The estimate of the energy confinement time indicates that the energy transport in the cold surrounding area is anomalously rapid.

There could be two reasons of anomalous transport: turbulent transport caused by the RF heating and the enhancement of transport due to defects of the stellarator magnetic configuration. Within the frame of the turbulent transport hypothesis it is difficult to explain why the transport is so different in the kernel and surrounding area. The plasma heating proceeds in the kernel area efficiently and the RF field must be present there, but the anomalous transport is absent. Moreover, the peaking of the temperature in the centre is investigated in another RF heating scenarios at U-3M when the frame antenna was employed [18]. There the character of RF heating is different, but the electron temperature peaking is similar. The turbulent transport supposition does not explain why the location of the kernel hot zone does not depend on the plasma heating regime and is not sensitive to the discharge parameters.

A remaining suggestion is an imperfection of the magnetic configuration of U-3M. A calculated Poincare plot of the magnetic field lines in poloidal cross-section is shown in Figure 9.

The region of nested magnetic surfaces surrounds the magnetic axis and is restricted to $\langle r \rangle < 3$ cm. The surrounding area contains a chain of 3 big magnetic islands. Smaller islands are also present. Such a difference of the magnetic field topology in these two areas may provide different plasma confinement properties.

5. Magnetic configurations of Uragan-3M

A review of the studies on magnetic configuration of U-3M together with the corresponding references can be found in reference [1]. The standard configuration of U-3M (see Figure 9) is characterized by some undercompensation of the vertical magnetic field of the torsatron helical winding, so that the resulting vertical field B_v is of about 1.2 % of the toroidal field B_0. In this case the magnetic configuration turns out to be shifted toward the outer circumference of the torus. The advantage of this configuration is that it has the magnetic well and the improved plasma MHD stability.

Further studies however brought to light some disadvantages of the standard configuration of U-3M. In numerical calculations and experiments rather large magnetic islands corresponding to □= 1/4 were found (see in reference [1]) that can be explained by an influence of a small eccentricity in the vertical field coils. Besides, the increased neoclassical transport was calculated for this configuration (see in reference [19]) that can be a result of a fact that the standard configuration of U-3M is an outward-shifted configuration and is opposite to the inward-shifted configurations of the heliotron/torsatron devices, which are close to "sigma-optimized" configurations (see in references [20-22]). The calculations performed in reference [19] for the inward-shifted configuration of U-3M (see Figure 10) show significant improvement of the neoclassical transport as compared to the standard configuration (the inward-shifted configuration was obtained in case of opposite direction of the resulting vertical magnetic field, $B_v / B_0 = 1.2$ %).

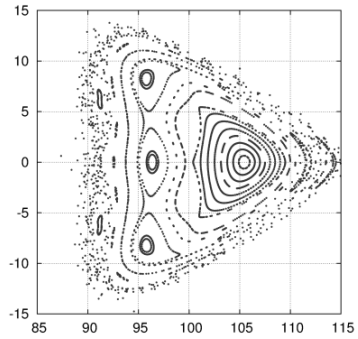

Figure 9. Poincare plot of the magnetic field lines in poloidal cross-section (standard magnetic configuration).

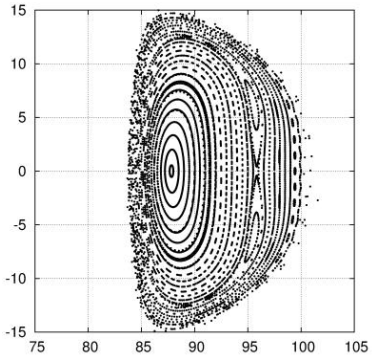

Figure 10. The same as in Figure 9 for inward shifted magnetic configuration.

From the viewpoint of MHD stability, the inward-shifted configurations seem to be less favorable than the outward-shifted ones because of a change in the magnetic well into the magnetic hill (see reference [1]). However, such a supposition is in conflict with the recent experimental findings for the Large Helical Device (LHD) summarized in reference [23]. From these LHD results, it follows that an inward-shifted configuration with a magnetic hill has better neoclassical confinement than outward-shifted configurations with a magnetic well. Also, from these results it follows that plasma with an average beta of 3 % is stable in the inward-shifted configuration, even though the theoretical stability conditions of Mercier modes and pressure-driven low-n modes are violated. So, it follows from reference [23] that MHD stability and good transport properties are compatible in the inward-shifted configuration. Besides, inward shifting of the plasma column could positively influence on the Pfirsch-Schluter current [24]. In calculations the inward-shifted configuration for Uragan-3M can be conveniently obtained by a certain increase of currents in the vertical field coils (approximately by 10 % as compared to the currents for the standard configuration).

6. Conclusions

Investigation of radial profiles of emissivity of different optical lines and ECE diagnostics results reveal two zones at Uragan-3M plasma column which have different electron temperatures and properties in plasma confinement. The central zone is restricted to $\langle r \rangle < 3$ cm. It is characterized by relatively high electron temperature that indicates good plasma confinement. A zone with cold electrons and worse confinement surrounds the hot plasma kernel and extends to the plasma edge, $\langle r \rangle = 12$ cm. The total electron temperature profile is too peaked to be explained by a central RF heating. The mostly plausible explanation is different rate of heat transport in these two zones. The outer zone dominates in volume and determines the global confinement characteristics such as the energy and particle confinement times that are below expected. The analysis of the Uragan-3M standard magnetic configuration indicates that the system of nested magnetic surfaces exists only in the central zone. There are some options to change the configuration so, that the area of the nested magnetic surfaces becomes wider. The inward-shifted magnetic configuration is a perspective choice in this respect.

Acknowledgements

This work has been carried out within the framework of the EUROfusion Consortium and has received funding from the Euratom research and training programme 2014-2018 under grant agreement No 633053. The views and opinions expressed herein do not necessarily reflect those of the European Commission.

Prof. O.S. Pavlichenko's comments are appreciated.

References

[1] Lesnyakov G G et al. 1992 *Nucl. Fusion* **32** 2157

[2] Shvets O M, Dikij I A, Kalinichenko S S et al. 1986 *Nucl. Fusion* **26** 23

[3] Moiseenko V E 1991 Alfvén Heating in Toroidal Plasmas by Using Three-Half- turn Loop Antenna IAEA Technical Committee Meeting. Proc. 8th Int.Workshop on Stellarators,Kharkov (IAEA, Vienna) 207.

[4] Dolgopolov V V and Stepanov K N 1965 Nucl. Fusion **5** 276

[5] Stadnik Yu S, Moiseenko V E, Stepanov K N et al. 2007 Theoretical Analysis of RF Plasma Production in Uragan-2M Torsatron *34th EPS Conf. on Plasma Phys.(Warsaw, 2-6 July 2007) (ECA vol 31F)* p 4.157

[6] Moiseenko V E, Stadnik Yu S, Lysoivan A I and Korovin V B 2013 *Plasma Phys. Rep.* **39** 873

[7] Lysojvan A I, Moiseenko V E, Shvets O M and Stepanov K N 1992 *Nuclear Fusion* **32** 1361

[8] Moiseenko V E, Berezhnyj V L, Bondarenko V N et al. 2011 2011 *Nucl. Fusion* **51** 083036

[9] Pavlichenko R O, Zamanov N V and Kulaga A E 2017 *Problems of Atomic Science and Technology. Series: Plasma Physics* **1** 257 (http://vant.kipt.kharkov.ua/ARTICLE/VANT_2017_1/article_2017_1_257.pdf)

[10] Pavlichenko R O, Kulaga A E, Zamanov N V, Pavlichenko O S 2011 *Problems of Atomic Science and Technology. Series: Plasma Physics* **1** 191 (http://vant.kipt.kharkov.ua/ARTICLE/VANT_2011_1/article_2011_1_191.pdf)

[11] Pavlichenko R O 2015 *Problems of Atomic Science and Technology. Series: Plasma Physics* **1** 293 (http://vant.kipt.kharkov.ua/ARTICLE/VANT_2015_1/article_2015_1_293.pdf)

[12] Zamanov N V, Pavlichenko R O, Kulaga A E 2016 *Problems of Atomic Science and Technology. Series: Plasma Physics* **6** 317 (http://vant.kipt.kharkov.ua/ARTICLE/VANT_2016_6/article_2016_6_317.pdf)

[13] Kuznetsov E I, Shcheglov D A Methods of high-temperature plasma diagnostics Moscow, Atomizdat, 1974. 160 p. In Russian.

[14] Pearce W J Extremely High Temperatures John Wiley & Sons, Inc., New York, 1958, p.123-134

[15] Bondarenko V N, Konovalov V G, Tsybenko S A, Voitsenya V S, Volkov E D2003 *Problems of Atomic Science and Technology. Series: Plasma Physics* **1** 23 (http://vant.kipt.kharkov.ua/ARTICLE/VANT_2003_1/article_2003_1_23.pdf)

[16] Fujimoto T, Sawada K and Tanaka K 1989 *J. Appl. Phys.* **66** 2315

[17] Voitsenya V S, Shapoval A N, Pavlichenko R O, Pankratov I M et al. 2014 *Phys. Scr.* **T161** 014009

[18] Pankratov I M, Beletskii A A, Berezhnyj V L, Burchenko P Ya et al. 2010 *Contrib. Plasma Phys.* 50 **6-7** 520–8

[19] Kalyuzhnyj V N and Nemov V V 2004 *Fusion Science and Technology* **46** 248

[20] Mynic H E, Chu T K and Boozer A H 1982 *Phys. Rev. Lett.* **48** 322

[21] Mynic H E 1983 *Phys.Fluids* **26** 1008

[22] Shaing K C and Hokin S A 1983 *Phys. Fluids* **26** 2136

[23] Motojima O et al. 2003 *Nucl. Fusion* **43** 1674

[24] Pustovitov V D 1996 *Nucl. Fusion* **36** 583.